



Trans. Nonferrous Met. Soc. China 24(2014) 3621-3631

Transactions of Nonferrous Metals Society of China

www.tnmsc.cn

Extrusion force analysis of aluminum pipe fabricated by CASTEX using expansion combination die

Fu-rong CAO¹, Jing-lin WEN¹, Hua DING¹, Zhao-dong WANG², Chuan-ping YU³, Fei XIA¹

- 1. School of Materials and Metallurgy, Northeastern University, Shenyang 110819, China;
- 2. State Key Laboratory of Rolling and Automation, Northeastern University, Shenyang 110819, China;
 - 3. Dandong Feituo Aluminum Products Co., Ltd., Dandong 118000, China

Received 24 November 2013; accepted 14 April 2014

Abstract: To determine the extrusion force of pipe fabricated by continuous casting and extrusion (CASTEX) using an expansion combination die, the metallic expansion combination die was divided into diversion zone, expansion zone, flow dividing zone, welding chamber, and sizing zone, and the corresponding stress formulae in various zones were established using the slab method. The deformation zones of CASTEX groove were divided into liquid and semisolid zone, solid primary gripping zone, and solid gripping zone, and the formulae of pipe extrusion forces were established. Experiments were carried out on the self-designed CASTEX machine to obtain the aluminum pipe and measure its extrusion force using the expansion combination die. The experimental results of radial extrusion force for aluminum pipe are in good agreement with the calculated ones.

Key words: continuous casting and extrusion; continuous extrusion; expansion combination die; aluminum pipe; stress analysis; extrusion force

1 Introduction

Unlike conventional extrusion [1,2] and other types of extrusion [3-5], CONFORM, continuous extrusion forming, turns the friction resistance between the billet and the container into the driving force of billet deformation. As long as various billets or feedstock such as rod, particles, and powders of aluminum, copper, and polymeric material are fed continuously into the entrance of CONFORM machine, a wide range of products such as wire, rod, profile, and tube that meet the requirements can be produced continuously at the exit of extrusion die. Since the appearance of CONFORM, its application in major industrial and scientific fields has been increasing. MITCHELL [6] pointed out that CONFORM was a commercially viable method of producing hollow sections and tubing for air conditioning, refrigeration and cable television applications. CHURCH [7] introduced the application of CONFORM to the production of sheathe cable and to the manufacture of various solid and hollow sections in Europe and put forward the development of an expansion chamber, leading to the die through which profile whose cross section was larger than that of the feedstock could be made. HAWKES and MORGAN [8] reported the CONFORM extrusion of copper or aluminum solid sections and the sheathing or cladding operations. LANGERWEGER and MADDOCK [9] and MADDOCK [10] changed the solid feedstock of CONFORM into molten metal and presented an innovative continuous casting and extrusion (CASTEX) machine with the expansion chamber. Although the idea of the expansion chamber was put forward, no report was available to produce real pipes in practical CASTEX process using an expansion combination die except Northeastern University in China. In recent years, RAAB et al [11] and XU et al [12] have explored the application of ECAP (equal channel angular pressing)-CONFORM to the fabrication of ultrafine-grained (UFG) aluminum wire and Al-6061 rod. Recently, FENG et al [13], YUN et al [14], and HE et al [15] have reported the continuous extrusion of Cu-0.16Cr-0.12Zr alloy, have investigated the continuous extrusion and rolling forming of copper strip, and achieved 200% elongation to failure at 473 K and 1×10^{-4} s⁻¹ in AZ31 magnesium alloy processed by ECAP-CONFORM, respectively.

Foundation item: Projects (51334006, 50274020) supported by the National Natural Science Foundation of China Corresponding author: Fu-rong CAO; Tel: +86-24-83670183; E-mail: cfr-lff@163.com DOI: 10.1016/S1003-6326(14)63507-X

The theoretical mechanics analysis and simulation on CONFORM or CASTEX process using finite element (FEM) simulation, upper bound method, slab method, and slip line method have been increasing. First, FEM simulation was carried out. PENG et al [16] predicted the processes of defect initiation and development during CONFORM process. KIM et al [17] investigated the effects of several process parameters, such as material flow, defect occurrence, temperature and effective strain distribution, on the process characteristics. CHO and JEONG [18] addressed a parametric investigation on the occurrence of the surface defect in CONFORM process using FEM simulation. YUN et al [19] and WEI et al [20] investigated the metallic flow, strain field and temperature field of UFG copper rod using continuous ECAP, simulated the deformation behavior of continuous ECAP and investigated the effect of die angle and contact friction on the strain and stress distribution, flow homogeneity, shear deformation and torque, respectively, by FEM method. ZHAO et al [21] investigated the process of aluminum sheath during continuous extrusion using FEM simulation. Second, upper bound analyses were conducted. CAO et al [22] and KIM et al [23] derived the upper bound driving power equation for the CASTEX and the CONFORM processes, respectively. Third, slab method was used to determine the extrusion force. TIROSH et al [24] established a unit pressure distribution equation of CONFORM extrusion for wire. SHI et al [25] got a formula of CASTEX force for aluminum-steel cladding wire. SONG et al [26] established a formula of CONFORM extrusion force for copper bar. CAO et al [27] derived a formula of CONFORM expanding extrusion force for Al-5Ti-1B alloy and pure aluminum solid sections. Fourth, SEGAL [28] utilized the slip line method to study the mechanics of continuous ECAP of rectangular billets.

In terms of aforementioned application and theoretical analysis, the authors developed a CASTEX process with the expansion combination die so that the pipe with cross section larger than that of the feedstock was produced, and the corresponding equipment and relevant tools were designed. According to literature survey, there was little information available reporting on the mechanics analysis of aluminum pipe processed by CASTEX extrusion using the slab method. In this work, by using the expansion combination die designed by ourselves, the CASTEX process was divided into several deformation zones and the extrusion stress formulae were derived zone by zone. On the basis of wheel groove force analysis, the tangential force and radial force of driving the wheel groove for the CASTEX process were determined. Experiments were carried out on the self-designed CASTEX machine to obtain aluminum pipes and to compare the experimental force with the calculated one.

2 Mechanics analysis of CASTEX process using expansion combination die

The schematic diagram of the CASTEX equipment using the expansion combination die is shown in Fig. 1. Molten metal flows from the entrance of extruding wheel into the extrusion cavity formed by the wheel groove and the grip segment. Under the action of friction forces imposed by the two sides of wheel groove and the bottom surface, the molten metal solidifies, is deformed in the extrusion cavity and extruded out of the extrusion die to obtain the pipe product in required shape and properties, as shown in Fig. 2.

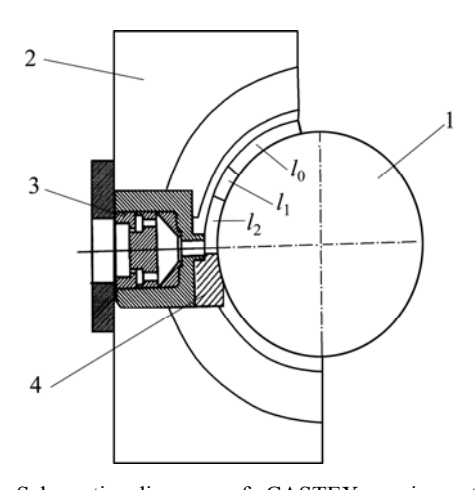


Fig. 1 Schematic diagram of CASTEX equipment using expansion combination die: l_0 —Liquid and semisolid zone; l_1 —Solid primary gripping zone; l_2 —Solid gripping zone; 1—CASTEX wheel; 2—Shoe; 3—Expansion combination die; 4—Abutment

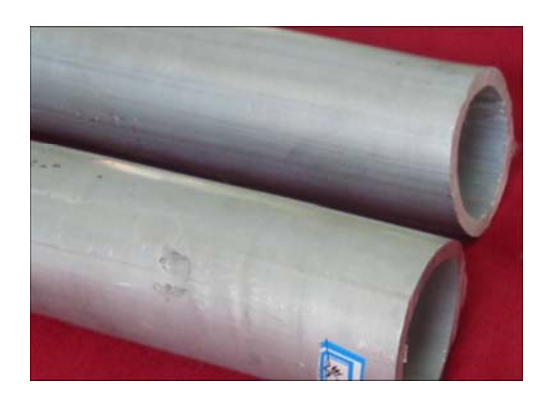


Fig. 2 Aluminum pipes produced by CASTEX using expansion combination die

According to the deformation characteristics of feedstock, the solidification and deformation processes in the wheel groove are divided into three deformation zones: liquid and semisolid zone l_0 , solid primary

gripping zone l_1 and solid gripping zone l_2 ; the deformation process in the expansion combination die is divided into five deformation zones: 1) diversion zone, 2) expansion zone, 3) flow dividing zone, 4) welding chamber, and 5) sizing zone, as shown in Fig. 3. Mechanics analysis was carried out zone by zone from the beginning of the sizing zone of the die to the wheel entrance.

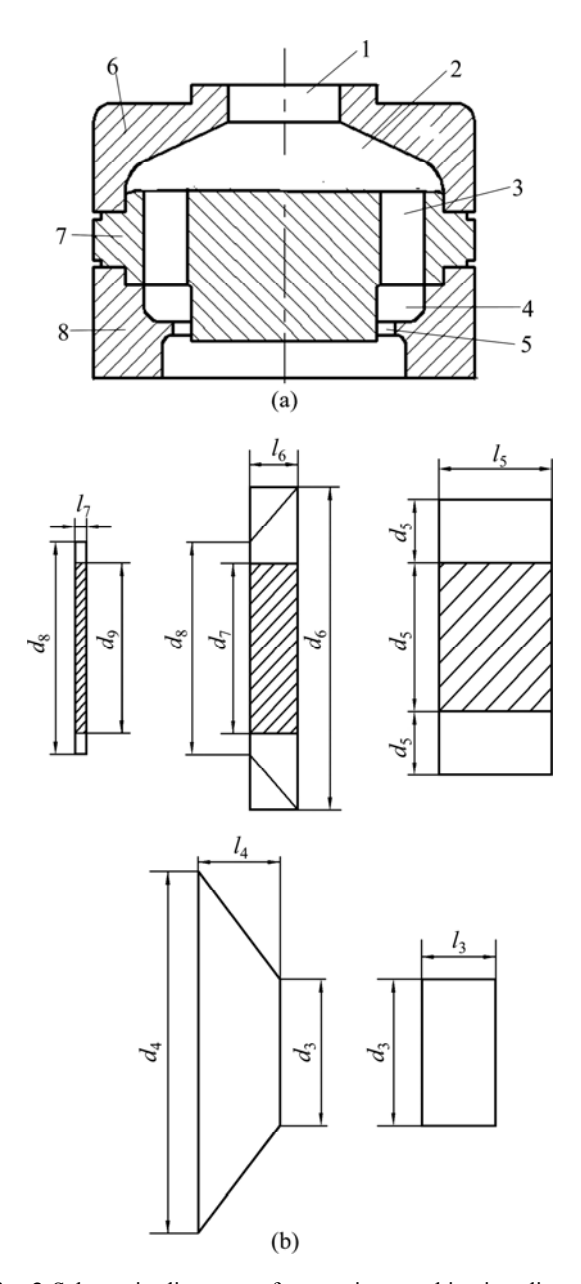


Fig. 3 Schematic diagrams of expansion combination die and its structure dimensions: (a) Schematic diagram of expansion combination die: 1—Diversion zone; 2—Expansion zone; 3—Flow dividing zone (four kidney holes); 4—Welding chamber; 5—Sizing zone; 6—Expanding die; 7—Male die; 8—Female die; (b) Structure dimensions of expansion combination die: From left to right, in turn dimensions of sizing zone, welding chamber, flow dividing zone, expansion zone, and diversion zone

2.1 Sizing zone

The stress analysis in the sizing zone is shown in Fig. 4. σ'_n and σ_n are normal pressures acting on the internal and external surfaces of the sizing zone of the die, respectively. σ'_n is the normal pressure of the rigid die acting on the metal. σ_n is the normal stress caused by the recovery of elastic deformation force. σ'_n and σ_n are assumed to be approximately equal to σ_s , the yield stress, i.e., $\sigma'_n = \sigma_n \approx \sigma_s$. Because of relative movement between the billet and the sizing zone of the die, friction stress occurs. τ' and τ are friction stresses acting on the internal and external surfaces of the sizing zone of the die, respectively, and abide by Coulomb's law of friction. The coefficients of friction on the internal and external surfaces in the sizing zone of the die are assumed to be f_{τ} :

$$\tau' = \tau = f_7 \sigma_n = f_7 \sigma_s \tag{1}$$

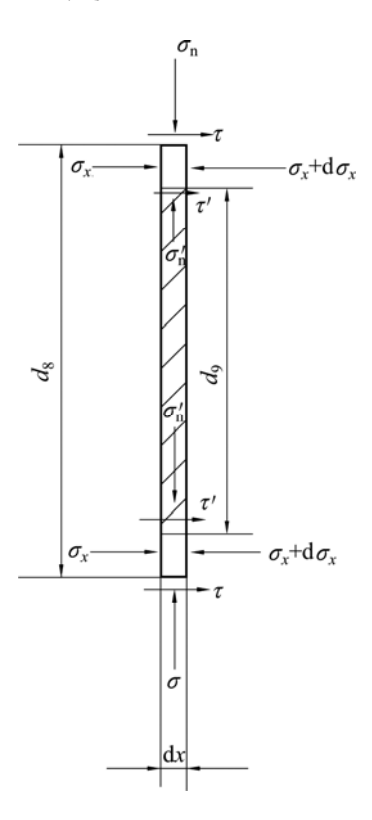


Fig. 4 Stress acting on infinitesimal element of sizing zone

The differential equation of static force equilibrium for the infinitesimal element along horizontal x axis direction is

$$(\sigma_x + d\sigma_x) \frac{\pi}{4} (d_8^2 - d_9^2) - \sigma_x \frac{\pi}{4} (d_8^2 - d_9^2) - f_7 \sigma_n \pi d_8 dx - f_7 \sigma'_n \pi d_9 dx = 0$$
 (2)

Equation (2) reduces to

$$(d_8 - d_9) d\sigma_x = 4f_7 \sigma_s dx \tag{3}$$

It is assumed that the stress acting on the boundary

between the sizing zone and the welding chamber is σ_7 . Based on the boundary condition, when x=0, $\sigma_x=0$; when $x=l_7$, $\sigma_x=\sigma_7$.

Definite integral of Eq. (3) becomes

$$\int_0^{\sigma_7} (d_8 - d_9) d\sigma_x = 4 \int_0^{l_7} f_7 \sigma_s dx$$

Above equality reduces to

$$\sigma_7 = \frac{4f_7\sigma_{\rm s}l_7}{d_8 - d_9} \tag{4}$$

where f_7 is the coefficient of friction between the billet and the sizing zone of die, σ_s is the flow stress of the material, l_7 is the length of the sizing zone of the die, d_8 is the diameter of the sizing zone of the die, and d_9 is the diameter of mandril.

2.2 Welding chamber

The stresses acting on the infinitesimal element of the welding chamber are shown in Fig. 5. σ'_n and σ_n are normal pressures acting on the internal and external surfaces of the welding chamber of the die, respectively. $\sigma'_n = \sigma_n \cos \alpha_1$ and $t' = f'\sigma'_n = f\sigma_n \cos \alpha_1$, where the semicone angle $\alpha_1 = \arctan[(d_6 - d_8)/(2l_6)]$ can be obtained according to the force equilibrium along vertical direction. For simplification, it is assumed that the normal pressures acting on the internal and external surfaces are approximately equal, $\sigma'_n \approx \sigma_n$, and their coefficients of friction are also the same. The shear stresses acting on the boundary between the movable

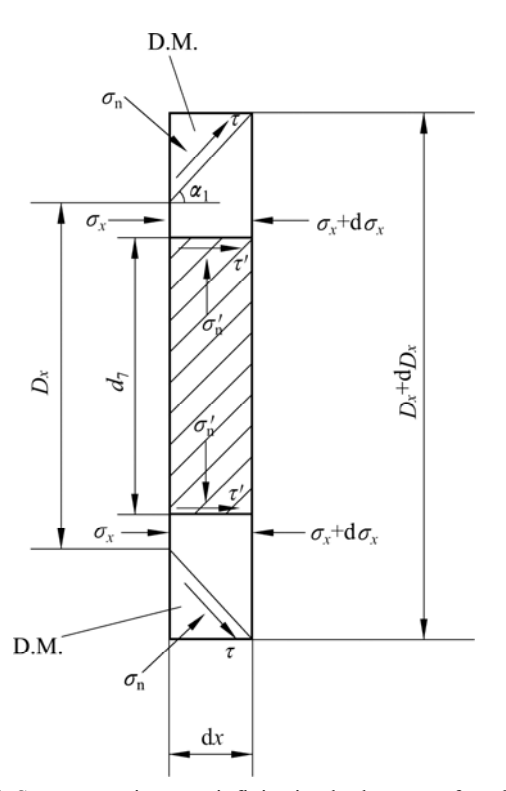


Fig. 5 Stresses acting on infinitesimal element of welding chamber

metal and the "dead" metal (D.M.) zone attain the maximum values. The coefficients of friction obey $f' = f = 1/\sqrt{3}$.

The differential equation of force equilibrium for the infinitesimal element along horizontal x axis direction is

$$(\sigma_{x} + d\sigma_{x}) \frac{\pi}{4} [(D_{x} + dD_{x})^{2} - d_{7}^{2}] - \sigma_{x} \frac{\pi}{4} [D_{x}^{2} - d_{7}^{2}] - \sigma_{n} (\pi D_{x} dx / \cos \alpha_{1}) \sin \alpha_{1} - \sigma_{s} \pi D_{x} dx / \sqrt{3} - \sigma_{s} \pi d_{7} dx / \sqrt{3} = 0$$
(5)

Neglecting differential quantities of the second order, in consideration of $dD_x/2 = (dx)tg\alpha_1$, Eq. (5) reduces to

$$2\sigma_x D_x dD_x + D_x^2 d\sigma_x - d_7^2 d\sigma_x - 2\sigma_n D_x dD_x - \frac{2\sigma_s}{\sqrt{3}\tan\alpha_1} D_x dD_x - \frac{2}{\sqrt{3}\tan\alpha_1} \sigma_n d_7 dD_x = 0$$
 (6)

Substituting Tresca's yield criterion, σ_n – σ_x = σ_s , into Eq. (6) leads to

$$(D_x^2 - d_7^2) d\sigma_x - 2D_x \left\{ \sigma_s \left[1 + \frac{\cot \alpha_1}{\sqrt{3}} + \frac{\cot \alpha_1}{\sqrt{3}} \frac{d_7}{D_x} \right] + \sigma_x \frac{\cot \alpha_1}{\sqrt{3}} \frac{d_7}{D_x} \right\} dD_x = 0$$

$$(7)$$

Let $\cot \alpha_1 / \sqrt{3} = B$, Eq. (7) becomes

$$(D_x^2 - d_7^2) d\sigma_x - 2D_x \{ \sigma_s [1 + B(1 + \frac{d_7}{D_x})] + \sigma_x B \frac{d_7}{D_x} \} dD_x = 0$$
(8)

Rearranging Eq. (8) yields

$$\frac{d\sigma_x}{dD_x} - \frac{2Bd_7}{D_x^2 - d_7^2}\sigma_x = \frac{2D_x\sigma_s(1+B) + 2B\sigma_sD_7}{D_x^2 - d_7^2}$$
(9)

Let

$$P(D_x) = \frac{2Bd_7}{D_x^2 - d_7^2},$$

$$2D_x \sigma_s(1+B) + 2Bc$$

$$Q(D_x) = \frac{2D_x \sigma_{\rm s}(1+B) + 2B\sigma_{\rm s}D_7}{D_x^2 - d_7^2}$$

Therefore,

$$\sigma_x = \exp[-\int P(D_x) dD_x] \cdot \{ \int Q(D_x) \exp[-\int P(D_x) dD_x] dD_x + C \}$$
 (10)

where *C* is a constant of integration.

Solving the above formula gives

$$\sigma_{x} = \left(\frac{D_{x} - d_{7}}{D_{x} + d_{7}}\right)^{B} \left[\int \frac{2\sigma_{s}(1+B)(D_{x} + d_{7})^{B}}{(D_{x} - d_{6})^{B+1}} dD_{x} + \right]$$

$$\frac{\sigma_{\rm s}}{B} (1 + \frac{2d_7}{D_x - d_7})^B + C$$
 (11)

It is assumed that the stress acting on the boundary between the welding chamber and the flow dividing zone is σ_6 . Based on the boundary condition, when $D_x=d_8$, $\sigma_x=\sigma_7$; when $D_x=d_6$, $\sigma_x=\sigma_6$.

Equation (11) reduces to

$$\sigma_{6} = \left(\frac{d_{6} - d_{7}}{d_{6} + d_{7}}\right)^{B} \cdot \left\{ \sigma_{7} \left(\frac{d_{8} + d_{7}}{d_{8} - d_{7}}\right)^{B} + \right.$$

$$\int_{d_{7}}^{d_{4}} \frac{2\sigma_{s} (1 + B)(D_{x} + d_{7})^{B}}{(D_{x} - d_{7})^{B+1}} dD_{x} +$$

$$\left. \frac{\sigma_{s}}{B} \left[(1 + \frac{2d_{7}}{d_{6} - d_{7}})^{B} - (1 + \frac{2d_{7}}{d_{8} - d_{7}})^{B} \right] \right\}$$

$$(12)$$

In Eq. (12), numerical integration for the second item shall be implemented to gain the calculated results.

2.3 Flow dividing zone

Flow dividing zone consists of four holes in kidney shape, as shown in Fig. 6. The flow dividing hole in kidney shape is assumed to be equivalent to a rectangle whose side lengths are h_5 and b_5 . The depth of the hole is equal to l_5 . Friction stress is determined according to the maximum shear stress. The coefficient of friction is assumed to be $f = 1/\sqrt{3}$. It is assumed that $\sigma'_n = \sigma_n \approx \sigma_s$, where σ'_n and σ_n are the normal pressures.

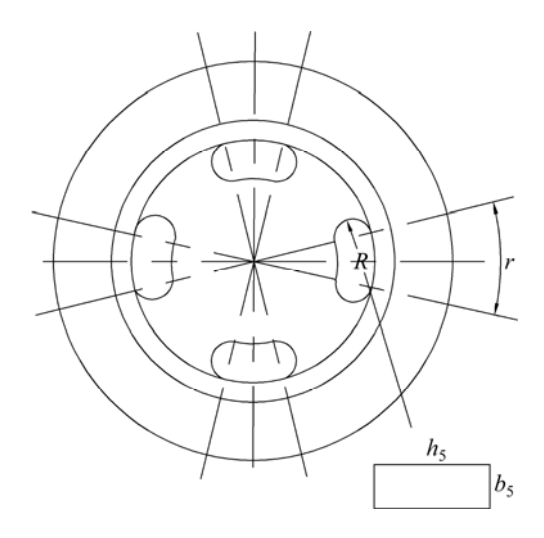


Fig. 6 Four flow dividing holes in male die of combination die

As shown in Fig. 7, the differential equation of force equilibrium for the infinitesimal element along horizontal *x* axis direction is

$$4(\sigma_x + d\sigma_x)b_5h_5 - 4\sigma_x b_5h_5 - 4 \times 2f\sigma_n h_5 dx = 0$$
 (13)

$$d\sigma_x = \frac{2}{\sqrt{3}b_5}\sigma_s dx \tag{14}$$

It is assumed that the stress acting on the boundary between the flow dividing zone and the expansion zone is σ_5 and the length of flow dividing zone is l_5 . Based on the boundary condition, when x=0, $\sigma_x=\sigma_6$; when $x=l_5$, $\sigma_x=\sigma_5$.

Definite integral of Eq. (12) becomes

$$\int_{\sigma_6'}^{\sigma_5} d\sigma_x = \frac{2}{\sqrt{3}b_5} \sigma_s \int_0^{l_5} dx$$
 (15)

Therefore,

$$\sigma_5 = \sigma_6 + \frac{2}{\sqrt{3}} \frac{l_5}{b_5} \sigma_s \tag{16}$$

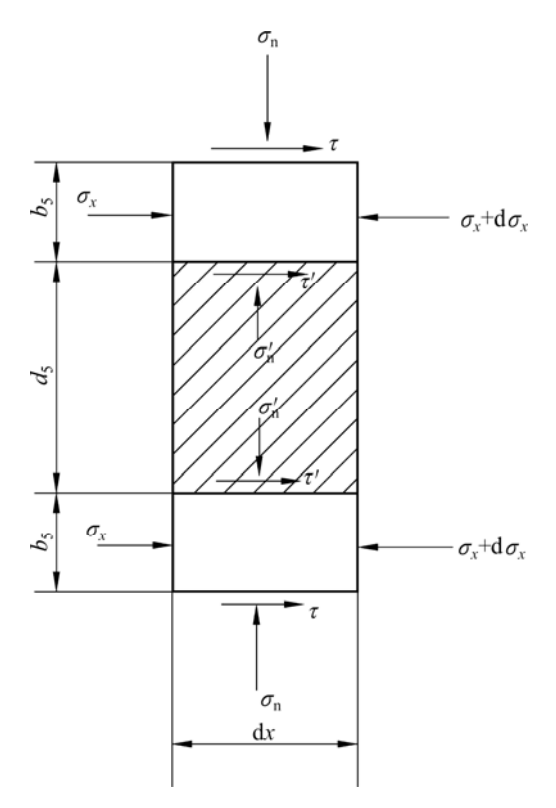


Fig. 7 Stress acting on infinitesimal element of flow dividing

2.4 Expansion zone

The infinitesimal element to be chosen is shown in Fig. 8. The shear stress, τ , acting on the boundary between the metal and the die reaches the maximum value, $\tau = \sigma_{\rm s}/\sqrt{3}$, and the coefficient of friction $f = 1/\sqrt{3}$. The differential equation of force equilibrium for the infinitesimal element along horizontal x axis direction is

$$(\sigma_x + d\sigma_x)\frac{\pi}{4}(D_x + dD_x)^2 - \sigma_x\frac{\pi}{4}D_x^2 - \sigma_x\frac{\pi}{4}D_x^2 - \sigma_x\frac{\pi}{4}D_xdx/\cos\alpha_2\sin\alpha_2 - \sigma_x\pi D_xdx/\sqrt{3} = 0$$
 (17)

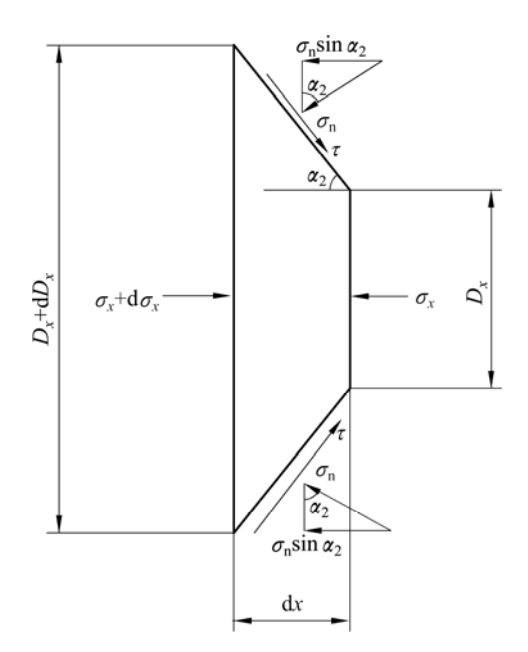


Fig. 8 Stress acting on infinitesimal element of expansion zone

Neglecting differential quantities of the second order, in consideration of $dD_x/2 = (dx)\tan\alpha_2$, Eq. (17) reduces to

$$\frac{\pi D_x}{4} (D_x d\sigma_x + 2\sigma_x dD_x) - \frac{1}{2} \sigma_n \pi D_x dD_x - \frac{\sigma_s}{\sqrt{3}} \frac{\pi D_x}{2 \tan \alpha_2} dD_x = 0$$
 (18)

Hence

$$2\sigma_{s}dD_{x} + D_{x}dD_{x} - 2\sigma_{n}dD_{x} - \frac{2\sigma_{s}}{\sqrt{3}}\frac{dD_{x}}{\tan\alpha_{2}} = 0$$

Substituting Tresca's yield criterion, $\sigma_n - \sigma_x = \sigma_s$, into above formula leads to

$$D_x d\sigma_x - 2\sigma_s dD_x - \frac{2\sigma_s}{\sqrt{3}} \cot \alpha_2 dD_x = 0$$

Hence,

$$d\sigma_x = 2\sigma_s (1 + \frac{1}{\sqrt{3}} \cot \alpha_2) \frac{dD_x}{D_x}$$
 (19)

It is assumed that the stress acting on the boundary between the expansion zone and the diversion zone is σ_4 . Based on the boundary condition, when $D_x=d_4$, $\sigma_x=\sigma_5$; when $D_x=d_3$, $\sigma_x=\sigma_4$.

Definite integral of Eq. (19) becomes

$$\int_{\sigma_5}^{\sigma_4} d\sigma_x = \int_{d_4}^{d_3} 2\sigma_s (1 + \frac{1}{\sqrt{3}} \cot \alpha_2) \frac{dD_x}{D_x}$$
 (20)

Because

$$\sigma_4 > \sigma_5, \int_{\sigma_5}^{\sigma_4} d\sigma_x > 0;$$
 $d_3 < d_4,$

$$\int_{d_4}^{d_3} 2\sigma_{\rm s} (1 + \frac{1}{\sqrt{3}} \cot \alpha_2) \frac{{\rm d}D_x}{D_x} < 0$$

The limit of integration on the right of equality sign is reversed and becomes

$$\int_{\sigma_5}^{\sigma_4} d\sigma_x = \int_{d_3}^{d_4} 2\sigma_s \left(1 + \frac{1}{\sqrt{3}} \cot \alpha_2\right) \frac{dD_x}{D_x}$$
 (21)

Therefore,

$$\sigma_4 = \sigma_s + 2\sigma_s (1 + \frac{1}{\sqrt{3}} \cot \alpha_2) \ln(d_4/d_3)$$
 (22)

where the semicone angle $\alpha_2 = \arctan[(d_4 - d_3)/(2l_4)]$.

2.5 Diversion zone

The infinitesimal element to be chosen is shown in Fig. 9. The shear stress, τ , acting on the boundary between the metal and the die reaches the maximum value, $\tau = f\sigma_{\rm n} = \sigma_{\rm s}/\sqrt{3}$. The differential equation of force equilibrium for the infinitesimal element along horizontal x axis direction is

$$(\sigma_x + d\sigma_x) \frac{\pi}{4} d_3^2 - \sigma_x \frac{\pi}{4} d_3^2 - \frac{1}{\sqrt{3}} \sigma_n \pi d_3 dx = 0$$
 (23)

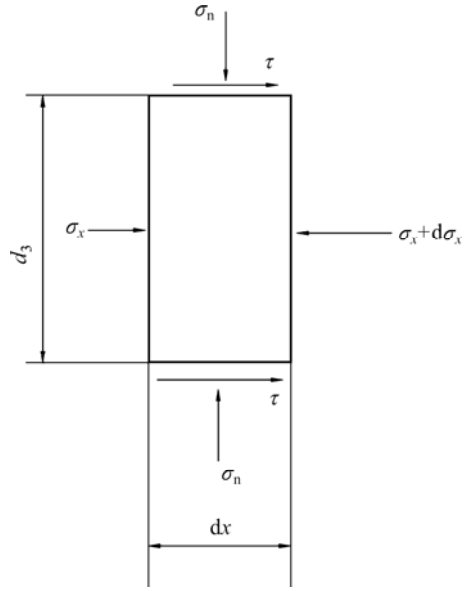


Fig. 9 Stress acting on infinitesimal element of diversion zone

Equation (23) reduces to

$$d_3 d\sigma_x = \frac{4}{\sqrt{3}} \sigma_s dx \tag{24}$$

Hence

$$d\sigma_x = \frac{4}{\sqrt{3}d_3}\sigma_s dx \tag{25}$$

It is assumed that the stress acting on the boundary between the diversion zone and the solid gripping zone is σ_3 and the length of diversion zone is l_3 . Based on the

boundary condition, when x=0, $\sigma_x=\sigma_4$; when $x=l_3$, $\sigma_x=\sigma_3$. Definite integral of Eq. (25) becomes

$$\int_{\sigma_4}^{\sigma_3} d\sigma_x = \frac{4}{\sqrt{3}d_3} \sigma_s \int_0^{l_3} dx$$
 (26)

Therefore,

$$\sigma_3 = \sigma_4 + \frac{4l_3}{\sqrt{3}d_3}\sigma_s \tag{27}$$

2.6 Liquid and semisolid zone, solid primary gripping zone and solid gripping zone

2.6.1 Lengths and stress distribution of liquid and semisolid zone, solid primary gripping zone and solid gripping zone

The deformation zones along the wheel groove are divided into liquid and semisolid zone l_0 , the solid primary gripping zone l_1 and solid gripping zone l_2 , as shown in Fig. 10(a). The distribution of friction stress τ

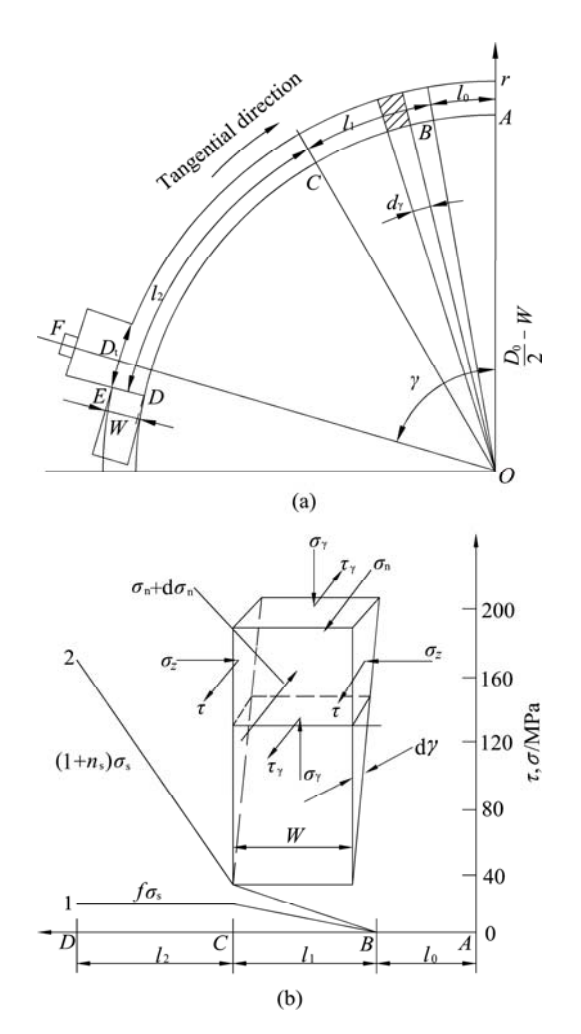


Fig. 10 Division of metallic solidification and deformation zones along wheel groove and stress distribution diagram: (a) Division of metallic solidification and deformation zones along wheel groove; (b) Distribution of friction stress τ and tangential stress σ_n in wheel groove (1—Friction stress τ ; 2—Tangential stress σ_n)

and tangential stress σ_n in the wheel groove is shown in Fig. 10(b).

1) Length of zone l_0

Liquid metal is poured into the groove and dynamic solidification occurs when friction stress τ =0 and tangential stress σ_n =0. The length of l_0 obeys

$$l_0 = (\frac{D_0}{2} - W)\gamma - l_1 - l_2 + \frac{D_t}{2}$$
(28)

where D_0 is the wheel diameter, W is the groove height or width, l_1 is the length of solid primary gripping zone, l_2 is the length of solid gripping zone, D_t = d_3 , and γ is the wrapping angle in rad.

2) Length of l_1 zone

Metal fills the groove gradually. τ starts from zero and increases till $f\sigma_s$; σ_n , the tangential stress, starts from zero and increases till σ_s , as shown in Fig. 10(b). The metal in section B-C is taken as the stress body. The metal in this section is subjected to the friction forces on both sides of the wheel groove and the tangential force is transferred from the front metal. The friction force of the groove bottom acting on the metal counteracts that of the grip segment acting on the metal in section B-C.

It is assumed that the friction stress in the section B-C is τ_1 , so $\tau_1 = f\sigma_s l/l_1$, which satisfies the boundary condition of l=0, $\tau_1=0$; $l=l_1$, $\tau_1=f\sigma_s$. Due to the simultaneous action of friction forces on both sides of the wheel groove, the friction force of the wheel groove acting on the stress body becomes

$$2\int_{0}^{l_{1}} \tau_{1} W dl = 2\int_{0}^{l_{1}} (f\sigma_{s} l/l_{1}) W dl = \frac{2}{l_{1}} \int_{0}^{l_{1}} f\sigma_{s} W l dl$$
 (29)

The tangential force is

$$\sigma_{\rm n}W^2 = \sigma_{\rm s}W^2 \tag{30}$$

Static force equilibrium of section B-C gives

$$\frac{2}{l_1} \int_0^{l_1} f \sigma_s W l dl = \sigma_s W^2$$
 (31)

Therefore,

$$l_1 = W / f \tag{32}$$

where f is the coefficient of friction and f=0.5.

3) Length of zone l_2

 τ is equal to $f\sigma_s$. Tangential stress σ_n in front of the abutment increases, causing the metal to change the flow direction and the extrusion stress produced in the extrusion direction to reach σ_3 which is required by extruding the metal in the expansion combination die out. Let $n_s = \sigma_3/\sigma_s$, the metal in section C-D is taken as the stress body. The metal in this section is subjected to the friction forces on both sides of the wheel groove and the tangential force σ_n is transferred from the abutment. The friction force of the groove bottom acting on the metal

counteracts that of the grip segment acting on the metal in section C-D.

The tangential force equilibrium in section C-D gives

$$2\int_{0}^{l_2} f\sigma_s W dl = \sigma_n W^2 - \sigma_s W^2$$
(33)

According to Tresca's yield criterion of maximum shear stress,

$$\sigma_{\rm n} - \sigma_{\rm 3} = \sigma_{\rm s} \tag{34}$$

Substituting $f = 1/\sqrt{3}$, Eq. (34), and $n_s = \sigma_3/\sigma_s$ into Eq. (33) gives

$$l_2 = \frac{\sqrt{3}}{2} n_{\rm s} W \tag{35}$$

$$\sigma_{\rm n} = (1 + n_{\rm s})\sigma_{\rm s} \tag{36}$$

2.6.2 Determination of CASTEX extrusion force

The CASTEX extrusion force means the tangential force, $P_{\rm t}$, and the radial force, $P_{\rm r}$, sustained by the wheel groove of CASTEX wheel. The wheel is taken as the force body. For the convenience of presentation, the force diagram of the wheel groove is shown in Fig. 11. The size of cross section of the groove is $W \times W$.

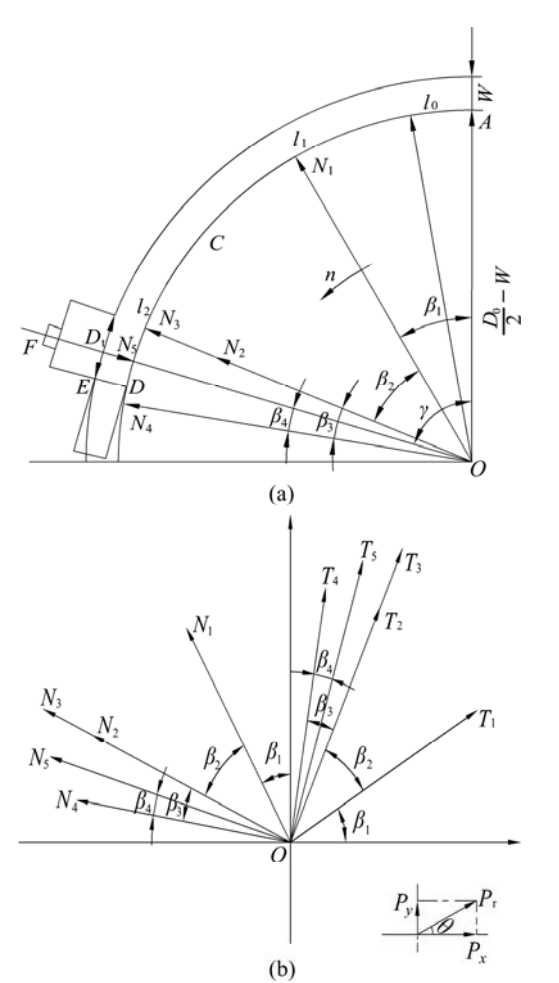


Fig. 11 Force diagrams of wheel groove for CASTEX extrusion

The forces acting on the side faces and the bottom surface of l_1 zone (acting on the middle point of l_1) are

$$T_1 = f\sigma_s W l_1 + \frac{1}{2} f\sigma_s W l_1, \quad N_1 = \frac{1}{2} \sigma_s W l_1$$
 (37)

The forces acting on the side faces and the bottom surface of l_2 zone (acting on the middle point of l_2) are

$$T_2 = 3f\sigma_{\rm s}Wl_2 , \quad N_2 = \sigma_{\rm s}Wl_2 \tag{38}$$

The flash forces caused by the clearance or gap (acting on the middle point of l_2) are

$$T_3 = 2bf\sigma_s l_2, \quad N_3 = 2b\sigma_s l_2 \tag{39}$$

The flash forces on the three sides of the abutment (acting on the middle point of Z) are

$$T_4 = 3f\sigma_s WZ , \quad N_4 = \sigma_s WZ \tag{40}$$

The forces of diversion zone acting on the wheel groove are

$$T_5 = fN_5, \quad N_5 = \sigma_3 \frac{\pi}{4} D_t^2$$
 (41)

where b is the length of single side flash and Z is the length of flash caused by the leakage between the abutment and the wheel groove.

Thus, the tangential force of deformation material acting on the wheel groove is

$$P_{t} = f\sigma_{s}Wl_{1} + \frac{1}{2}f\sigma_{s}Wl_{1} + 3f\sigma_{s}Wl_{2} + 2bf\sigma_{s}l_{2} + 3f\sigma_{s}WZ + \frac{\pi}{4}f\sigma_{3}D_{t}^{2}$$
(42)

The radial force of deformation material acting on the wheel center, $P_{\rm r}$, is determined by the following relation:

$$P_{\rm r} = \sqrt{P_{\rm x}^2 + P_{\rm y}^2} \tag{43}$$

$$\theta = \arctan \frac{P_y}{P} \tag{44}$$

where P_x is the horizontal component, P_y is the vertical component, and θ is the direction angle.

Resolution of forces is carried out for Fig. 11(b) and leads to

$$\begin{bmatrix} P_{xi} \\ P_{vi} \end{bmatrix} = \begin{bmatrix} -\sin \beta_i \cos \beta_i \\ \cos \beta_i \sin \beta_i \end{bmatrix} \begin{bmatrix} N_i \\ T_i \end{bmatrix}, i=1, 2, 3, 4, 5$$
 (45)

Combining the above formulae for i, horizontal component, P_x , and vertical component P_y , of radial force, P_T , are obtained.

$$P_x = -N_1 \sin \beta_1 - (N_2 + N_3) \sin(\beta_1 + \beta_2) -$$

$$N_{4} \sin(\gamma + \beta_{4}) - N_{5} \sin \gamma + T_{1} \cos \beta_{1} +$$

$$(T_{2} + T_{3}) \cos(\beta_{1} + \beta_{2}) + T_{4} \cos(\gamma + \beta_{4}) + T_{5} \cos \gamma$$

$$(46)$$

$$P_{y} = N_{1} \cos \beta_{1} + (N_{2} + N_{3}) \cos(\beta_{1} + \beta_{2}) +$$

$$N_{4} \cos(\gamma + \beta_{4}) + N_{5} \cos \gamma + T_{1} \sin \beta_{1} +$$

$$(T_{2} + T_{3}) \sin(\beta_{1} + \beta_{2}) + T_{4} \sin(\gamma + \beta_{4}) + T_{5} \sin \gamma$$

$$(47)$$

As actual directions of stress vectors are opposite to those shown in Fig. 11(b), it is necessary to add a minus sign before P_x and P_y and final P_x and P_y are obtained:

$$\begin{split} P_x &= N_1 \sin \beta_1 + (N_2 + N_3) \sin(\beta_1 + \beta_2) + \\ &\quad N_4 \sin(\gamma + \beta_4) + N_5 \sin \gamma - T_1 \cos \beta_1 - \\ &\quad (T_2 + T_3) \cos(\beta_1 + \beta_2) - T_4 \cos(\gamma + \beta_4) - T_5 \cos \gamma \\ P_y &= -N_1 \cos \beta_1 - (N_2 + N_3) \cos(\beta_1 + \beta_2) - \\ &\quad N_4 \cos(\gamma + \beta_4) - N_5 \cos \gamma - T_1 \sin \beta_1 - \\ &\quad (T_2 + T_3) \sin(\beta_1 + \beta_2) - T_4 \sin(\gamma + \beta_4) - T_5 \sin \gamma \ (49) \end{split}$$
 where
$$\beta_1 = [\pi(0.5D_0 - W) - 2l_1 - 2l_2 + D_t]/(D_0 - 2W) \ ,$$

$$\beta_2 = (l_1 + l_2)/(D_0 - 2W) , \quad \beta_3 = (l_2 + Z)/(D_0 - 2W) ,$$

$$\beta_4 = (D_t + Z)/(D_0 - 2W) , \quad \gamma = \beta_1 + \beta_2 + \beta_3 - \beta_4 .$$

These angles are determined according to the geometrical relation.

Equations (42), (43), (44), (48) and (49) are the derived formulae for radial CASTEX extrusion.

3 Experimental process and calculated results

3.1 Experimental process and results

CASTEX tests of aluminum pipes were conducted on the self-designed CASTEX machine with the expansion combination die. The wheel diameter was 300 mm. Liquid metal at 710 °C was poured into the rotary extrusion wheel groove and a pipe with a dimension of d50 mm×5 mm was obtained by extruding deformation. In the shoe, a sensor was mounted at the outlet side of the extrusion die to measure the radial force. Prior to the measurement of the radial force, the sensor was calibrated by a model DY-15 stabilized voltage power supply, a model YD-15 dynamic electrical resistance strain gauge and a model SC-16 light ray recording oscillograph on the universal tensile test machine. Thermocouples were inserted into the holes drilled on the grip segments and an X-Y four point temperature measuring device was used to measure the deformation temperature. The temperature that metal entered the die was measured to be 400 °C. According to WEN [29], the flow stress, σ_s , of aluminum at deformation temperature of 400 °C and strain rate of 3.07 s⁻¹ was 23.4 MPa and the coefficient of Coulomb's friction, f_7 , was 0.275.

3.2 Calculated results

The technical parameters of CASTEX machine and extrusion process are shown in Table 1.

Table 1 Technical parameters of CASTEX machine and extrusion process

D/mm	W/mm	t/°C	$\dot{\varepsilon}/s^{-1}$	f_7	$\sigma_{\rm s}$ /MPa	γ/(°)
300	10	400	3.07	0.275	23.4	90

The structure dimensions of the expansion combination die corresponding to Fig. 3(b) are shown in Table 2.

Table 2 Structure dimensions of expansion combination die (mm)

-							
	d_3	d_4	d_5	d_6	d_7	d_8	d_9
	34	84	50	76	40	50	40
	l_3	l_4	l_5	l	6	l_7	b_5
	18	20	28	13	5.5	3	15

The calculated stresses in various deformation zones and the comparison of the calculated extrusion radial force with the experimental one are shown in Table 3. The experimental radial force is in good agreement with the calculated one with an error of less than 10% under the present experimental condition.

Table 3 Calculated stresses in various deformation zones and comparison of the calculated extrusion radial force with the experimental one

σ ₃ /MPa	σ_4 /MPa	σ ₅ /MPa	σ_6 /MPa	σ_7 /MPa
253.93	225.32	163.44	113.03	7.72
$P_{\rm t}/{ m N}$	$P_{\rm r}/{\rm N}$	Ţ	$P_{\rm r}^{1)}/{\rm N}$	Error/%
237443	41740)6	459698	9.2

¹⁾ Experimental radial force.

4 Conclusions

- 1) An expansion combination die for the CASTEX process is designed. The metallic expansion combination die is divided into diversion zone, expansion zone, flow dividing zone, welding chamber, and sizing zone. The corresponding stress formulae in various zones are established using the slab method.
 - 2) The deformation zones of CASTEX groove are

divided into liquid and semisolid zone, solid primary gripping zone, and solid gripping zone. The formulae of pipe extrusion forces are established.

3) Experiments were carried out on the self-designed CASTEX machine to obtain the aluminum pipe and measure its extrusion force using the expansion combination die. The experimental results of radial extrusion force for aluminum pipe are in good agreement with the calculated ones.

References

- LI Jing-yuan, XIE Jian-xin, JIN Jun-bing, WANG Zhi-xiang. Microstructural evolution of AZ91 magnesium alloy during extrusion and heat treatment [J]. Transactions of Nonferrous Metals Society of China, 2012, 22(5): 1028–1034.
- [2] HAGHIGHAT H, MAHDAVI M M. Analysis and FEM simulation of extrusion process of bimetal tubes through rotating conical dies [J]. Transactions of Nonferrous Metals Society of China, 2013, 23(11): 3392–3399.
- [3] YING Tao, HUANG Jian-ping, ZHENG Ming-yi, WU Kun. Influence of secondary extrusion on microstructures and mechanical properties of ZK60 Mg alloy processed by extrusion and ECAP [J]. Transactions of Nonferrous Metals Society of China, 2012, 22(8): 1896–1901.
- [4] LIN Jin-bao, WANG Qu-dong, LIU Man-ping, CHEN Yong-jun, ROVEN H J. Finite element analysis of strain distribution in ZK60 Mg alloy during cyclic extrusion and compression [J]. Transactions of Nonferrous Metals Society of China, 2012, 22(8): 1902–1906.
- [5] GUAN Ren-guo, ZHAO Zhan-yong, CHAO Run-ze, LIAN Chao, WEN Jing-lin. Simulation of temperature field and metal flow during continuous semisolid extending extrusion process of 6201 alloy tube [J]. Transactions of Nonferrous Metals Society of China, 2012, 22(5): 1182–1189.
- [6] MITCHELL K J. Tube manufacture by the conform process [J]. Metallurgia, 1982, 8(9): 448–449.
- [7] CHURCH F L. Extrusion goes continuous: Process promises economies [J]. Modern Metals, 1984, 40(11): 34–40.
- [8] HAWKES D J, MORGAN R E. Conform extrusion [J]. Wire Industry, 1991, 58(6): 323–326.
- [9] LANGERWEGER J, MADDOCK B. Production of aluminum wire directly from the molten metal [J]. Wire World International, 1986, 28(11–12): 179–181.
- [10] MADDOCK B. Aluminum rod and other products by conform [J]. Wire Industry, 1987, 54(12): 728-731.
- [11] RAAB G J, VALIEV R Z, LOWE T C, ZHU Y T. Continuous processing of ultrafine grained Al by ECAP-CONFORM [J]. Materials Science and Engineering A, 2004, 382(1-2): 30-34.
- [12] XU C, SCHROENER S, BERBON P B, LANGDON T G. Principles of ECAP-CONFORM as a continuous process for achieving grain refinement: Application to an aluminum alloy [J]. Acta Materialia, 2010, 58(4): 1379–1386.
- [13] FENG Hui, JIANG Hai-chang, YAN De-sheng, RONG Li-jian. Effect of continuous extrusion on the microstructure and mechanical properties of a CuCrZr alloy [J]. Materials Science and Engineering A, 2013, 582: 219–224.

- [14] YUN Xin-bing, YOU Wei, ZHAO Ying, LI Bing, FAN Zhi-xin. Continuous extrusion and rolling forming velocity of copper strip [J]. Transactions of Nonferrous Metals Society of China, 2013, 23(4): 1108–1113
- [15] HE You-liang, GAO Fei, SONG Bao-yun, FU Rong, WU Gui-ming, LI Jian, JIANG Lan. Grain refinement of magnesium alloys by CONFORM: A continuous severe plastic deformation route? [J]. Materials Science Forum, 2012, 706–709: 1781–1786.
- [16] PENG Ying-hong, RUAN Xue-yu, ZUO Tie-yong. Defect prediction during CONFORM process by FEM [J]. Journal of Materials Processing Technology, 1994, 45: 539–543.
- [17] KIM Y H, CHO J R, JEONG H S, KIM K S, YOON S S. A study on optimal design for CONFORM process [J]. Journal of Materials Processing Technology, 1998, 80–81: 671–675.
- [18] CHO J R, JEONG H S. Parametric investigation on the surface defect occurrence in CONFORM process by the finite element method [J]. Journal of Materials Processing Technology, 2000, 104(3): 236–243.
- [19] YUN Xin-bing, SONG Bao-yun, CHEN Li. Ultra-fine grain copper prepared by continuous equal channel angular press [J]. The Chinese Journal of Nonferrous Metals, 2006, 16(9): 1563–1569. (in Chinese)
- [20] WEI Wei, ZHANG Wei, WEI Kun-xia, ZHONG Yi, CHENG Gang, HU Jing. Finite element analysis of deformation behavior in continuous ECAP process [J]. Materials Science and Engineering A, 2009, 516: 111–118.
- [21] ZHAO Ying, SONG Bao-yun, YUN Xin-bing, PEI Jiu-yang, JIA Chun-bo, YAN Zhi-yong. Effect of process parameters on sheath forming of continuous extrusion sheathing of aluminum [J]. Transactions of Nonferrous Metals Society of China, 2012, 22(2): 3073–3080.
- [22] CAO Fu-rong, SHI Zhi-yuan, WEN Jing-lin. Upper-bound approach analysis of driving power of wheel for CASTEX [J]. Transactions of Nonferrous Metals Society of China, 1999, 9(1): 99–104.
- [23] KIM Y H, CHO J R, KIM K S, JEONG H S, YOON S S. A study of the application of upper bound method to the CONFORM process [J]. Journal of Materials Processing Technology, 2000, 97(3): 153–157.
- [24] TIROSH J, GROSSMAN G, GORDAN G. Theoretical and experimental study of the CONFORM metal forming process [J]. Journal of Engineering for Industry: Trans ASME, 1979, 101(2): 116–120.
- [25] SHI Zhi-yuan, CAO Fu-rong, CHEN Yan-bo, WEN Jing-lin. The analysis and study of the CASTEX force of AS wire [J]. Journal of Materials Processing Technology, 1999, 86(1–3): 115–118.
- [26] SONG Bao-yun, SONG Na-na, CHEN Li. Analysis of continuous extrusion extending forming force for wide copper bus-bar [J]. Journal of Plasticity Engineering, 2011, 18(4): 6–10. (in Chinese)
- [27] CAO Fu-rong, WEN Jing-lin, DING Hua, WANG Zhao-dong, LI Ying-long, GUAN Ren-guo, HOU Hui. Force analysis and experimental study of pure aluminum and Al-5%Ti-1%B alloy continuous expansion extrusion forming process [J]. Transactions of Nonferrous Metals Society of China, 2013, 23(1): 201–207.
- [28] SEGAL V M. Mechanics of continuous equal-channel angular extrusion [J]. Journal of Materials Processing Technology, 2010, 210(3): 542–549.
- [29] WEN Jing-lin. Metallic extrusion and drawing technology [M]. Shenyang: Northeastern University Press, 1996: 57–59. (in Chinese)

扩展组合模连续铸挤铝管材的挤压力分析

曹富荣1,温景林1,丁桦1,王昭东2,于传平3,夏飞1

- 1. 东北大学 材料与冶金学院, 沈阳 110819;
- 2. 东北大学 轧制技术与连轧自动化国家重点实验室, 沈阳 110819;
 - 3. 丹东飞拓铝品有限公司, 丹东 118000

摘 要:为了确定管材扩展组合模连续铸挤过程的变形力,将金属扩展组合模的模腔划分为导流区、扩展区、分流区、焊合区和定径区,分析各区金属的受力状态;用切块法建立各区应力计算公式。将金属连续铸挤型腔划分为液相区与半固态区、固态初始夹紧区和固态夹紧区,建立管材连续铸挤挤压力计算公式。在自行设计的连续铸挤机上进行铝管扩展组合模连续铸挤实验并测量其挤压力,获得的径向挤压力实验结果与理论计算结果吻合。关键词:连续铸挤;连续挤压;扩展组合模;铝管;应力分析;挤压力

(Edited by Wei-ping CHEN)